MESOSTRUCTURED MATERIALS

Electrochemical characterization of Pt/carbon xerogel and Pt/carbon aerogel catalysts: first insights into the influence of the carbon texture on the Pt nanoparticle morphology and catalytic activity

Nathalie Job · Frédéric Maillard · Julien Marie ·
Sandrine Berthon-Fabry · Jean-Paul Pirard ·
Marian Chatenet

Abstract Platinum catalysts were prepared by impregnation/reduction of two carbon supports with different pore textures: one carbon aerogel and one carbon xerogel. Impregnation with H_2PtCl_6 was followed by reduction in aqueous phase with $NaBH_4$, filtration, drying and subsequent reduction by H_2. The catalysts were characterized by widely used physico-chemical methods (N_2 adsorption, transmission electron microscopy, X-ray diffraction and CO chemisorption); from these techniques, no significant difference could be detected between the two samples. Actual Pt surface areas measured by coulometry of the electrochemical CO_{ads} stripping are comparable for both samples. However, the peak position and charge below each electrooxidation peak points towards different fraction of small/large particles within these two samples. In addition, CO_{ads} stripping shows that a fraction of the Pt particle surface is not electrochemically active. Pronounced differences observed in the specific activity towards O_2 reduction reaction were then explained by structural differences in Pt particles, undetectable by physico-chemical characterization techniques.

N. Job (✉) · J.-P. Pirard
Laboratoire de Génie Chimique (B6a), Université de Liège, 4000 Liège, Belgium
e-mail: Nathalie.Job@ulg.ac.be

F. Maillard · M. Chatenet
Laboratoire d'Électrochimie et de Physico-chimie des Matériaux et des Interfaces (LEPMI), UMR 5631 CNRS/Grenoble-INP/UJF, BP75, 38402 St Martin d'Hères Cedex, France

J. Marie · S. Berthon-Fabry
Mines ParisTech, Centre Énergétique et Procédés, BP 207, 06904 Sophia-Antipolis Cedex, France

Introduction

Carbon xerogels and aerogels are texture-tailored carbons prepared by evaporative or supercritical drying of organic gels, such as resorcinol-formaldehyde (RF) aqueous gels for instance, followed by pyrolysis under inert atmosphere [1–3]. These very pure carbon materials have already been used for various applications, among which catalysis [4–6]. Compared to activated carbons or carbon blacks, one of the advantages of RF carbon gels is that their pore texture can be adjusted through an appropriate choice of the synthesis conditions [1–3]. As a consequence, it is possible to decrease, and even to suppress diffusional limitations often encountered with classical carbon-supported catalysts by choosing supports of adequate pore size range [5]. Recently, that kind of material was studied as a support to prepare Pt/C catalysts designed for H_2/air proton exchange membrane fuel cells (PEMFCs) [7–10]. Similar to what has been observed in gas phase catalysis, carbon aerogels and xerogels with appropriate pore texture enhance transport phenomena in the cathode catalytic layer [9].

In catalysis, the catalyst characterization is usually focused on the analysis of its composition, support texture/chemistry and metal dispersion. However, it is now well established that the structure of the metal nanoparticles, i.e. their size, crystallographic orientation and texture, strongly influences their electrocatalytic activity [11]. Methods frequently used in catalyst characterization such as transmission electron microscopy (TEM), chemisorption, or X-ray diffraction (XRD) are very useful but cannot always account for the observed differences in catalytic activity for a given reaction. In this ambit, electrochemical characterization by CO_{ads} stripping turns out to be very helpful to characterize the nanostructure of carbon-supported Pt particles [11–13]. CO_{ads} stripping voltammograms may be

considered as fingerprints of the particle size distribution and allows controlling the presence/absence of noble metal particle agglomerates. Indeed, the position of the CO_{ads} (electro)oxidation peak strongly depends on the mean particle size and is shifted towards positive potential with decreasing the Pt particle size [11]. Moreover, the presence of Pt agglomerates in Pt/C electrocatalysts features an additional peak in CO_{ads} stripping voltammogram, which is shifted 100 mV negative against that of Pt particles ca. 3–4 nm size [12, 13].

In this study, Pt/C catalysts with high metal loading (30–35 wt%) were prepared by impregnation of either a carbon xerogel or a carbon aerogel with different pore sizes and pore volumes. The samples were characterized by nitrogen adsorption–desorption, TEM, CO chemisorption and XRD. CO_{ads} stripping voltammograms were performed to unveil the structural differences between them. Finally, the activity of the Pt/C catalysts for the oxygen reduction reaction (ORR) was determined in aqueous acid electrolyte media. This study aims at determining the influence of the carbon texture on the Pt nanostructure, and the subsequent impact on the catalyst performances for the ORR. In particular, this study shows how electrochemical methods can advantageously complete widely used physico-chemical techniques for the characterization of heterogeneous catalysts.

Experimental

Support and catalyst preparation

Two carbon supports were chosen for this study: a carbon xerogel and a carbon aerogel. The materials were synthesized using procedures developed in previous studies with slight differences for the xerogel and the aerogel. Aqueous gels were first obtained by polycondensation of resorcinol with formaldehyde in water, in the presence of Na_2CO_3. The resorcinol/formaldehyde molar ratio, R/F, was fixed at 0.5, which is usually considered as the stoichiometric ratio [1–3]. In the case of the carbon xerogel, the resorcinol/sodium carbonate molar ratio, R/C, was fixed at 1000, whereas the solvents/(resorcinol + formaldehyde) molar ratio, D, was chosen equal to 5.7. Note that, in D, the term "solvents" includes not only the deionised water added, but also the water and methanol (stabilizer) present in the formaldehyde solution. In the case of the aerogel, R/C and D were chosen equal to 200 and 10, respectively, which corresponds to a gel formulation leading to a poorly porous material if the gel be dried by evaporation [3]. The complete synthesis procedure of the aqueous gels is fully described elsewhere (for xerogel, see [3]; for aerogel, see [7, 8]).

The wet materials were then dried, either by evaporation (xerogel) or supercritical drying (aerogel). The organic xerogel was dried at 60 °C, the pressure being reduced from 10^5 to 10^3 Pa over 2 days. The sample was then left at 150 °C (10^3 Pa) for 12 h. Finally, the carbon xerogel was obtained by pyrolysis at 800 °C during 2 h under nitrogen flow [3]. The aerogel was obtained by drying the wet gel under supercritical conditions after solvent exchanges (water to acetone, then acetone to CO_2) [8]. The dry organic aerogel was pyrolyzed at 1050 °C for 30 min under flowing nitrogen.

Pt/C catalysts were prepared by impregnation of these two carbon substrates. The impregnation procedure was previously used in the synthesis of Pt/carbon aerogel catalysts designed for the preparation of membrane-electrode assemblies of PEM fuel cells [7–10]. The nominal Pt/(Pt + C) mass ratio, Pt_n, was chosen equal to 0.35. Finely grinded carbon powder (xerogel or aerogel, 500 mg) was suspended in 450 mL of H_2PtCl_6 aqueous solution (0.6 g_{Pt} L^{-1}). At the beginning of the impregnation, the pH of the solution was in both cases about 2.2 due to the acidity of H_2PtCl_6. After 24 h of magnetic stirring, $NaBH_4$ was added to reduce the Pt ionic precursors into metallic Pt. Overstoichiometry of $NaBH_4$ versus Pt ensured the complete reduction of the platinum salt: indeed, during this operation, the reduction of water into H_2 also occurs, and competes with the Pt reduction process. Afterwards, the Pt-doped carbon powder was washed thoroughly with boiling water and filtered. After drying at 60 °C in air for 12 h, the catalysts were treated in flowing H_2 for 30 min at 350 °C to ensure the complete reduction of the Pt^{z+} species.

In the following, the catalysts are labelled as X-Pt (xerogel-supported catalyst) and A-Pt (aerogel-supported catalyst).

Physico-chemical characterization of the supports and catalysts

The pore texture of the supports and final catalysts was characterized by the combination of nitrogen adsorption–desorption, performed at 77 K with a Sorptomatic Carlo Erba 1900, and mercury porosimetry, performed with a Carlo Erba Porosimeter 2000. The analysis of the isotherms provided the BET-specific surface area, S_{BET}, the micropore volume calculated by the Dubinin–Radushkevich equation, V_{DUB}, and the total pore volume calculated from the adsorbed volume at saturation, V_p. Hg porosimetry enabled obtaining the pore volume corresponding to pores of width >7.5 nm, V_{Hg}. Since N_2 adsorption–desorption is applicable to the analysis of pores <50 nm in diameter, and Hg porosimetry is limited to pores >7.5 nm in diameter,

the total void volume, V_v, was obtained by combining both techniques [14]:

$$V_v = V_{DUB} + V_{cum < 7.5nm} + V_{Hg}, \qquad (1)$$

where $V_{cum<7.5nm}$ is the cumulative volume of pores of width between 2 and 7.5 nm determined by the Broekhoff-de Boer theory [15]. For samples containing micropores and mesopores only, the isotherm displays a plateau at saturation, and N_2 adsorption is sufficient for determining the total void volume: V_v and V_p are equal. Note that, in the case of catalysts, all the textural parameters were corrected to take into account the mass of Pt deposited: in other words, all parameters are expressed per mass unit of carbon, not of catalyst.

The bulk density of the two carbons, ρ_{bulk}, was determined by mercury pycnometry. Finally, the bulk density of the support after impregnation was obtained by correcting the value obtained from mercury pycnometry for the mass increase due to metal addition. Indeed:

$$\rho_{bulk} = \rho_{bulk,cat} \frac{(100 - Pt_{ICP})}{100}, \qquad (2)$$

where ρ_{bulk} is the bulk density of the carbon support, and $\rho_{bulk,cat}$ is the bulk density of the catalyst measured by mercury pycnometry.

The metal content of the catalysts after impregnation, drying and reduction was measured by Inductively Coupled Plasma-Atomic Emission Spectrometry (ICP-AES, Iris Advantage Thermo Jarrel Ash). The preparation of the Pt solutions from the catalysts is thoroughly described in a previous study [16]. To measure the size of the metal particles, the catalysts were investigated by TEM, with a Jeol 100 SX (80 kV) device. The samples were crushed and dispersed in ethanol and subsequently deposited on a copper grid. The metal particles were also analysed by XRD with a Siemens D5000 goniometer using the Cu-K$_\alpha$ line (Ni filter). The mean metal particle size, d_{XRD}, was estimated from Scherrer's equation [17].

Carbon monoxide chemisorption was used to determine the accessible Pt surface, $S_{CO-chem}$. In brief, a first CO adsorption isotherm was achieved to measure the total amount of adsorbed carbon monoxide (chemisorbed + physisorbed). The catalyst was then outgassed, and a second CO adsorption isotherm was measured to evaluate the amount of physisorbed CO. The total amount of chemisorbed CO was deduced by subtracting the second isotherm from the first one and extrapolating the nearly horizontal difference curve to the uptake axis. Isotherms were measured with a Fisons Sorptomatic 1990 equipped with a turbomolecular vacuum pump that allows reaching a high vacuum of 10^{-3} Pa. The entire procedure, from the sample preparation to the adsorption measurement, is fully described elsewhere [16].

Electrochemical characterization of the catalysts

Rotating disk electrode (EDT 101, Tacussel) experiments were carried out on a thin active layer (AL) of Pt/C catalyst deposited on a glassy carbon electrode. The AL was prepared from a suspension blended from 10 mg of catalyst, 200 mg of 5 wt.% Nafion® solution in alcohol (Aldrich), and 1 mL of ultrapure water (18.2 MΩ cm—3 ppb total organic compounds, Millipore Elix + Gradient). After homogenization in an ultrasonic bath for 1 h, 10 μL of the suspension was deposited on the electrode. This electrode (diameter = 5 mm) was previously polished with diamond paste down to 1 μm and washed for 15 min in three successive ultrasonic baths of acetone, ethanol–water (1:1) and water. The suspension deposited was then dried and sintered for 15 min at 150 °C in air to reconstitute the Nafion® and ensure the binding of the catalyst layer to the glassy carbon surface. In order to remove the air contained in the catalyst and to fill its porosity with electrolyte solution, a drop of H_2SO_4 1 M was deposited on the catalyst, and the electrode was then outgassed under vacuum until no air bubbles were visible.

All electrochemical measurements were carried out in sulphuric acid (1 M, suprapur-Merck) at 25 °C. The voltammetric experiments were performed using Autolab-PGSTAT20 potentiostat with a three-electrode cell and a saturated calomel electrode as reference (+0.245 V vs. normal hydrogen electrode, NHE). However, all the potentials are expressed on the NHE scale hereafter.

The catalysts were characterized by CO_{ads} stripping. The Pt surface was saturated with CO (N47, Alphagaz) by bubbling for 6 min in the solution; afterwards, the non-adsorbed CO was removed from the cell by Ar bubbling for 39 min. During the CO adsorption and Ar bubbling, the electrode was held at +0.095 V vs. NHE. Three voltammetric cycles were then recorded at 0.02 V s^{-1} between +0.045 and +1.245 V vs. NHE. The active area of platinum, $S_{CO-strip}$, was calculated assuming that the electrooxidation of a full monolayer of CO_{ads} requires 420×10^{-6} C cm$_{Pt}^{-2}$ [18].

To measure the activity of the catalysts, the ORR was performed after saturation of the electrolyte solution with oxygen. During the measurement, the O_2 concentration was kept at saturation by gentle O_2-bubbling. The quasi-steady-state voltammograms were recorded at 10^{-3} V s^{-1} from +1.095 to +0.245 V vs. NHE. In order to account for the reactants diffusion–convection in the liquid layer, the experiment was repeated at four RDE rotation speeds (42, 94, 168 and 262 rad s^{-1}) and the average mass-transport corrected intensity obtained from the four curves was used in the calculations [19]. To evaluate the catalyst activity towards oxygen reduction, three parameters were isolated: (i) the Tafel slope, b, (ii) the specific activity at 0.85 V vs.

NHE, SA$_{85}$ and (iii) the specific activity at 0.90 V vs. NHE, SA$_{90}$. These potentials correspond to 0.39 and 0.34 V ORR overpotentials in 1 M sulphuric acid, values classically monitored in a PEMFC cathode at low current densities (i.e. under kinetic control).

Results

Physico-chemical characterization of the supports and catalysts

The main textural data obtained from nitrogen adsorption and mercury porosimetry are gathered in Table 1. As expected from previous results [3], the pore texture of the two carbon supports is very different in the mesopore/macropore range (pore size > 2 nm). Indeed, the pore size distributions, micropores excluded, calculated from nitrogen adsorption and mercury porosimetry (Fig. 1) show that, in the case of the xerogel, the pore size ranges from 50 to 85 nm; the distribution is shifted down to 10–25 nm in the case of the aerogel. The pore volumes are also very different: 2.1 vs. 4.8 cm^3 g^{-1}, for the xerogel and the aerogel, respectively. The same remark applies to the bulk density values (ρ_{bulk} = 0.38 and 0.19 g cm^{-3} for the xerogel and the aerogel, respectively). The texture difference is exclusively due to the meso/macropore volumes, $V_{>2nm}$. Indeed, the void volume related to micropores (size < 2 nm) is similar (0.26 cm^3 g^{-1}) and this agrees with previous studies [3, 9]. Globally, carbon gels are composed of interconnected microporous spherical-like nodules, the size of which mainly depends on the pH of the RF solution [1–4]. The size of internodular voids, i.e. the mesopores and macropores, depends on both the nodule
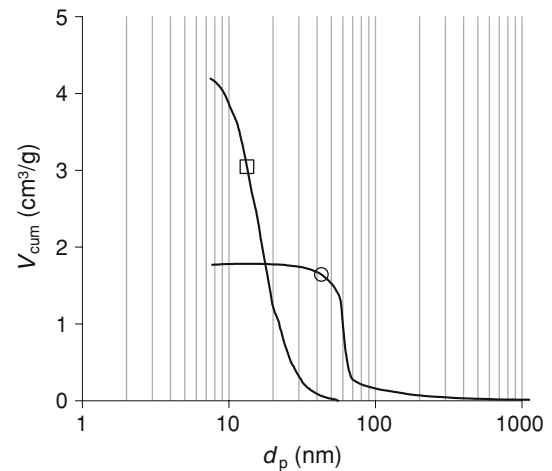
Fig. 1 Meso/macropore size distribution of the carbon supports: cumulative pore volume as a function of the pore size. (*circle*) Carbon xerogel; (*square*) carbon aerogel

size and the drying procedure [1–3]. As a consequence, two nanostructured carbon supports with completely different pore size distributions were easily prepared for the purpose of this study. Previous studies show that the pore size of carbon gels is fully controllable, from a few nanometres to a few micrometres, and in a large range of pore volume (0.5–7 cm^3 g^{-1}) [1–3].

Interestingly, both final catalysts display lower-specific surface area than the raw support (Table 1): S_{BET} decreases from about 600 down to ∼500 m^2 g^{-1}. The micropore volume decreases accordingly, from 0.26 to 0.22–0.23 cm^3 g^{-1}. On the contrary, the meso/macropore volume and size, as well as the bulk density, remain constant in each sample. The difference between the carbon supports and the catalysts is due to the blocking of some micropores by

Table 1 Synthesis variables of the gels and texture parameters of the initial carbon materials and carbon materials in the catalysts

	R/C (–)	D (–)	S$_{BET}$ (m^2 g^{-1}) ±5	V$_{DUB}$ (cm^3 g^{-1}) ±0.01	V$_{>2nm}$ (cm^3 g^{-1}) ±0.1	V$_v$ (cm^3 g^{-1}) ±0.1	d$_{p,min}$ (nm) ±5	d$_{p,max}$ (nm) ±5	ρ_{bulk} (g cm^{-3}) ±0.02
Supports									
Xerogel	1000	5.7	623	0.26	1.8	2.1	50[a]	85[a]	0.38
Aerogel	200	10	595	0.26	4.5	4.8	10[b]	25[b]	0.19
Catalysts									
X-Pt	1000	5.7	532	0.23	1.8	2.0	50[a]	85[a]	0.38
A-Pt	200	10	480	0.22	4.5	4.7	10[b]	25[b]	0.19

Note: All the parameters concerning the catalysts are related to the carbon support, metal excluded

R/C resorcinol/sodium carbonate molar ratio, *D* dilution ratio, *S*$_{BET}$ BET-specific surface area, *V*$_{DUB}$ micropore volume calculated from Dubinin–Radushkevich equation, *V*$_{>2nm}$ mesopore/macropore volume, *V*$_v$ total pore volume, *d*$_{p,max}$ maximum pore size, *d*$_{p,min}$ minimum pore size, ρ_{bulk} bulk density of the carbon (metal excluded in the case of the catalysts) determined by Hg pycnometry

[a] ±5 nm (obtained from mercury porosimetry measurements)

[b] ±2 nm (deduced from nitrogen adsorption)

metal particles; this effect was already observed with carbon xerogel-supported Pt catalysts prepared by another method [16]. The blocking is also confirmed from the calculation of the bulk density of the carbon in the catalysts: when corrected for the metal mass introduced during impregnation (Eq. 2), the bulk density of the support in the catalyst remains identical to that of the pristine carbon (Table 1: $\rho_{bulk} = 0.38$ and 0.19 g cm^{-3} for X-Pt and A-Pt, respectively). Since the bulk density of the support does not change after impregnation, the origin of the surface decrease is the blocking of some pores by metal particles.

Table 2 displays data obtained from the analysis of the catalysts by ICP-AES, XRD, CO chemisorption and TEM. ICP-AES shows that the actual Pt loading of the catalysts, Pt_{ICP}, is close to the nominal value, Pt_n (35 wt%): 31.0 and 34.9 wt% for X-Pt and A-Pt, respectively. Metal losses during the reduction and washing steps performed after impregnation are quite low. The proportion of metal located at the surface of the Pt particles, i.e. the dispersion, D_{Pt}, was calculated from [17]:

$$D_{Pt} = n_{s,m} M_{Pt} X_{Pt\text{-}CO} \times 10^{-3} \qquad (3)$$

where $n_{s,m}$ is the amount of CO needed to form a chemisorbed monolayer on surface Pt atoms (mmol g_{Pt}^{-1}) and M_{Pt} is the atomic weight of Pt (195.09 g mol^{-1}). $X_{Pt\text{-}CO}$ represents the chemisorption mean stoichiometry, i.e. the mean number of Pt atoms on which one CO molecule is adsorbed. In this study, $X_{Pt\text{-}CO}$ was chosen equal to 1 (i.e. linear bonding between Pt and CO), which is not straightforward due to a probable change of stoichiometry with the metal particle size in the case of very small diameters [20], but nevertheless enables comparing the X-Pt and A-Pt samples. Implications of the choice $X_{Pt\text{-}CO} = 1$ are discussed in the "Discussion" section. The metal dispersion is very similar: 16.3 and 15.2% for the xerogel- and aerogel-supported catalyst, respectively. A 'mean equivalent particle diameter', d_{CO}, i.e. the particle diameter leading to a metal surface equivalent to that detected by chemisorption, is obtained by [17]:

$$d_{CO} = \frac{6(v_m/a_m)}{D_{Pt}}, \qquad (4)$$

where v_m is the mean volume occupied by a metal atom in the bulk of a metal particle (for Pt: $v_m = 0.0151$ nm^3) and a_m is the mean surface area occupied by a surface metal atom (for Pt: $a_m = 0.0807$ nm^2). The obtained mean equivalent diameters equal 6.9 (X-Pt) and 7.4 nm (A-Pt). The total surface of the Pt particles, $S_{CO\text{-}chem}$, can be calculated from d_{CO} and the density of platinum, ρ_{Pt} (21.09 g cm^{-1}). Indeed:

$$S_{CO-chem} = 6\frac{V_{Pt}}{d_{CO}m_{Pt}} = 6\frac{1}{d_{CO}\rho_{Pt}}, \qquad (5)$$

where V_{Pt} and m_{Pt} are the volume and the mass of Pt present in the catalyst, respectively. $S_{CO\text{-}chem}$ is equal to 41 m^2 g_{Pt}^{-1} (X-Pt) and 39 m^2 g_{Pt}^{-1} (A-Pt).

Figure 2 shows the X-ray diffractograms of the two catalysts. Metal particle sizes calculated through Scherrer's equation, d_{XRD}, are found equal to 22 (X-Pt) and 18 nm (A-Pt); these values do not match at all those obtained by CO chemisorption, d_{CO}. This implies that the metal particle size distribution is not monodisperse: large and small particles should coexist, the smaller ones probably remaining undetected by XRD due to the high intensity of the peak corresponding to the large particles. This assumption is confirmed by TEM micrographs (Fig. 3). Two different families of particles are indeed observed by TEM: large particles (10–30 nm) are surrounded by smaller Pt clusters (2–7 nm). Therefore, two mean particle diameters, d_{TEM1} and d_{TEM2}, were calculated from a set of at least 60 particles for each particle family, selected from several catalyst grains (Table 2). Note that due to the size difference and to the fact that the small and large particles are not homogeneously dispersed onto the support, the evaluation of d_{TEM1} and d_{TEM2} had to be performed on two sets of micrographs with two different scales, which makes difficult the combination of both contributions. The size limit between the two families was fixed at 9 nm, which roughly corresponds to the less frequent particle size.

Table 2 Composition of the catalysts and Pt particle dispersion from ICP-AES, CO chemisorption, XRD and TEM

Catalyst	Pt_n (wt%)	ICP	CO chemisorption			XRD	TEM	
		Pt_{ICP} (wt%) ±0.1	D_{Pt} (%) ±0.5	d_{CO} (nm) ±0.5	$S_{CO\text{-}chem}$ (m^2 g_{Pt}^{-1}) ±1	d_{XRD} (nm) ±1	$d_{TEM,1}$ (nm) ±1	$d_{TEM,2}$ (nm) ±0.5
X-Pt	35.0	31.0	16.3	6.9	41	22	18	4.1
A-Pt	35.0	34.9	15.2	7.4	39	18	15	4.3

Pt_n nominal platinum loading, Pt_{ICP} actual platinum loading measured by ICP-AES, D_{Pt} platinum dispersion, d_{CO} equivalent Pt particle diameter calculated from CO chemisorption, $S_{CO\text{-}chem}$ Pt surface area detected by CO chemisorption, d_{XRD} Pt particle diameter obtained from XRD through Scherrer's law, $d_{TEM,1}$ mean Pt particle size for particles bigger than 7 nm in diameter obtained from TEM micrographs, $d_{TEM,2}$ mean Pt particle size for particles <7 nm in diameter obtained from TEM micrographs
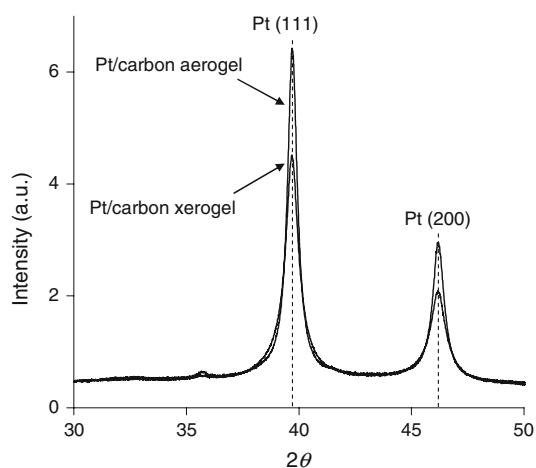
Fig. 2 X-ray diffractograms of the two catalysts

d_{TEM1} equals 18 and 15 nm, whereas d_{XRD} is 22 and 18 nm for the xerogel- and aerogel-supported catalyst, respectively. d_{TEM1} is slightly smaller than the crystallite size calculated from the X-ray diffractograms. However, since XRD is sensitive to the volume of particles, the diameter estimated from Scherrer's law is slightly overestimated when the particle size is not monodisperse: the mean crystallite size calculated from the peak broadening corresponds to a volume weighted average diameter $\sum n_i d_i^4 / n_i d_i^3$ [17], where n_i is the number of particles of diameter d_i. As a conclusion, XRD and TEM measurements match well for the group of the large particles (>9 nm). d_{CO} takes into account the existence of the smaller particles, the mean size of which, d_{TEM2}, is estimated to be 4.1 (X-Pt) and 4.3 nm (A-Pt) by TEM; d_{CO}, which takes into account both the large and small particles, is thus intermediate between d_{TEM1} and d_{TEM2}. d_{CO} is closer to d_{TEM2} because the surface developed by the small particles is much larger than that corresponding to the large ones.

Electrochemical characterization of the catalysts

Figure 4 shows the CO_{ads} voltammograms of the two catalysts. CO_{ads} electrooxidation on Pt proceeds through a Langmuir–Hinshelwood mechanism on Pt, which includes water dissociation into oxygen-containing species, recombination of the former species with CO, yielding CO_2 [11]. In contrast with the physico-chemical characterizations presented in the "Physico-chemical characterization of the supports and catalysts" section, the CO_{ads} stripping voltammograms show tremendous differences between the structures of the catalysts prepared on the two different supports.

CO_{ads} stripping voltammograms for X-Pt and A-Pt display three CO oxidation peaks centred at about +0.73, +0.81 and +0.92 V vs. NHE (0.020 V s^{-1}), the charge

below each peak being function of the sample investigated. As mentioned previously [11–13], the electrooxidation of a CO_{ads} monolayer is a structure-sensitive reaction and provides a wealth of information on the particle size distribution and the presence/absence of particle agglomeration. It has been reported that the position of the CO_{ads} stripping peak strongly depends on the mean particle size and is shifted towards positive potential with decreasing the Pt particle size (the reader is referred to [11–13] for more details). Taking into account a sweep rate dependence of 0.080 V dec^{-1} [13] and considering that the highest oxidation peak (at ca. 0.92 V vs. NHE) corresponds to CO_{ads} electrooxidation at small nanoparticles ($d < 1.9$ nm) and the lowest oxidation peak at ca. 0.81 V vs. NHE to the CO_{ads} electrooxidation at large particles ($d > 3.3$ nm) [11], comparison of the two different CO_{ads} stripping provides the following conclusions: the detected size distribution of A-Pt is mostly composed of large (3–4 nm) particles, whereas that of X-Pt is composed of small Pt particles (≤ 2 nm). Finally, the peak located at +0.73 V vs. NHE in the CO_{ads} stripping highlights the presence of Pt particle aggregates, the proportion of which is greater for A-Pt than X-Pt [12, 13]. These observations remarkably parallel the TEM analysis: aggregates are visible in both samples (Fig. 3a″, b″). For example, an aggregate of three Pt crystallites is highlighted by a black square in Fig. 3a″.

Interestingly, the Pt surfaces detected by CO_{ads} stripping ($S_{CO\text{-strip}}$ = 32 and 29 m^2 g$_{Pt}^{-1}$ for X-Pt and A-Pt, respectively, Table 3) are about 25% lower than those obtained by CO chemisorption ($S_{CO\text{-chem}}$ = 41 and 39 m^2 g$_{Pt}^{-1}$, Table 2). This agrees with a maximum CO_{ads} coverage of ca. 0.7 observed for single crystals and polycrystalline Pt in electrochemistry: indeed, according to Gomez et al. [21], θ_{CO} for Pt(111), Pt(100) and Pt(110) equals 0.64 and 0.82 and 0.82, respectively.

Oxygen reduction reaction

Oxygen reduction voltammograms obtained between +1.095 and +0.245 V vs. NHE were used to determine the electrocatalytic activity of the two catalysts. The kinetic current density, i_k, which includes the correction for the mass-transport in the so-called diffusion layer in the liquid electrolyte, was calculated at the relevant potentials (0.85 and 0.90 V vs. NHE) from [19]:

$$i_k = \frac{ii_l}{i_l - i}, \tag{6}$$

where i is the measured current density and i_l is the limiting current density [19]. The Tafel slopes of the ORR were drawn by fitting the Tafel plots (i.e. E vs. $\log(i_k)$) of the kinetic current density measurements between +0.95 and +0.80 V vs. NHE (Fig. 5). For the comparison of the two
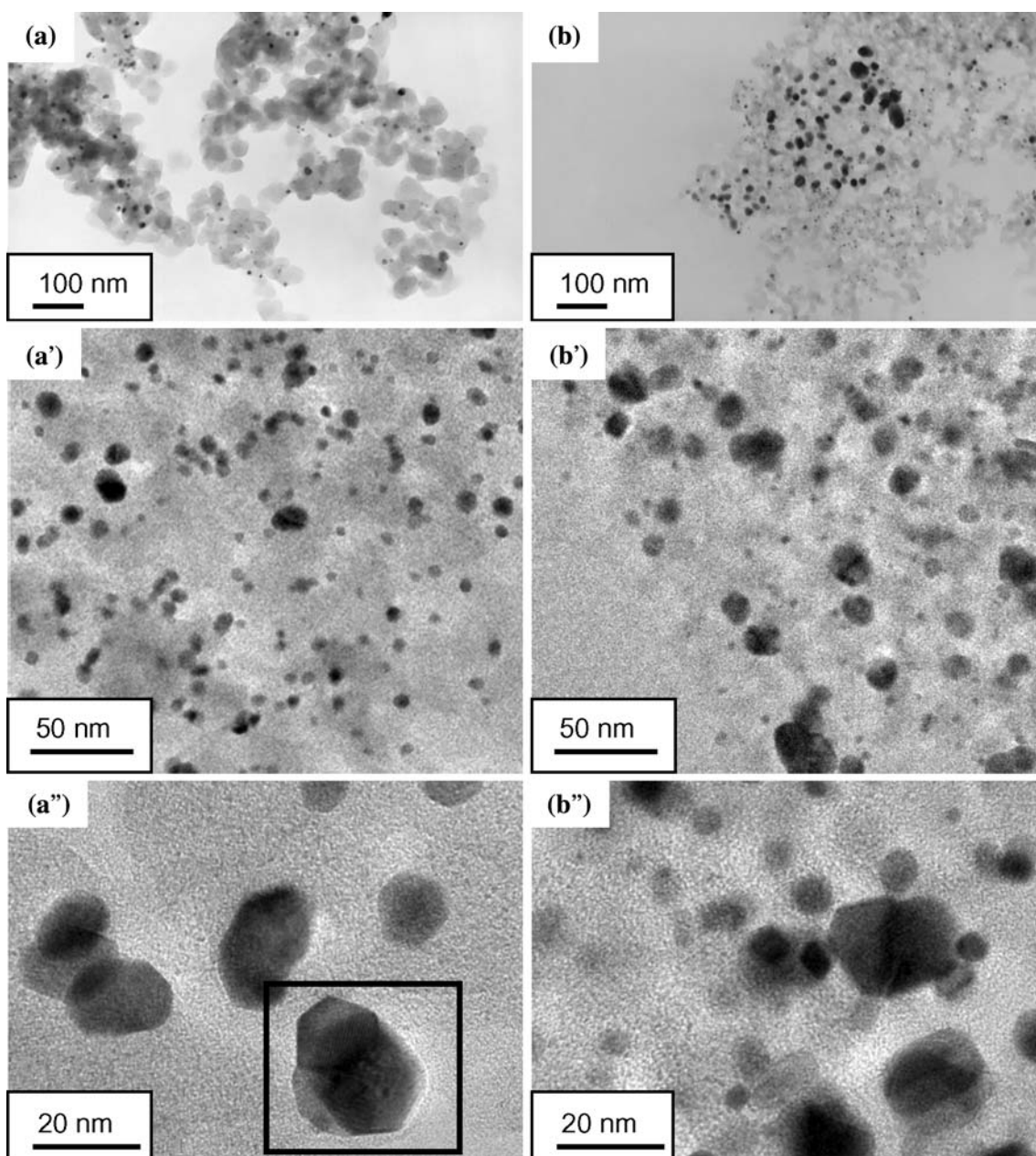
Fig. 3 Examples of TEM micrographs of the two catalysts at various scales. **a** Pt/carbon xerogel and **b** Pt/carbon aerogel. Micrographs (**a″**) and (**b″**) highlight the presence of Pt particle aggregates in both catalysts: the *black square* (**a″**) shows an aggregate of three Pt crystallites

catalysts, the specific activities (SA) are calculated at 0.85 and 0.90 V vs. NHE by normalizing i_k to the platinum active area detected by CO_{ads} stripping, $S_{CO-strip}$ (Table 3).

Both catalysts display Tafel slopes corresponding to values generally reported in the literature for ORR on carbon black-supported nanoparticles [22, 23], considering a classical mechanism involving four electrons per O_2 molecule (i.e. ~ -0.070 V dec^{-1}): b is found equal to -0.071 and -0.067 V dec^{-1} for X-Pt and A-Pt, respectively (Table 3). Nevertheless, one can observe that the aerogel-supported catalyst, A-Pt, is more active than its xerogel-supported counterpart, X-Pt: the specific activities

obtained for A-Pt are higher than those observed with X-Pt. For example, the specific activity obtained at 0.85 V with A-Pt $\left(SA_{85} = 29.0 \; \mu A \; cm_{Pt}^{-2}\right)$ is ca. 50% higher than for X-Pt $\left(SA_{85} = 19.9 \; \mu A \; cm_{Pt}^{-2}\right)$ $SA_{90} = 5.1$ and $3.9 \; \mu A \; cm_{Pt}^{-2}$ for A-Pt and X-Pt, respectively.
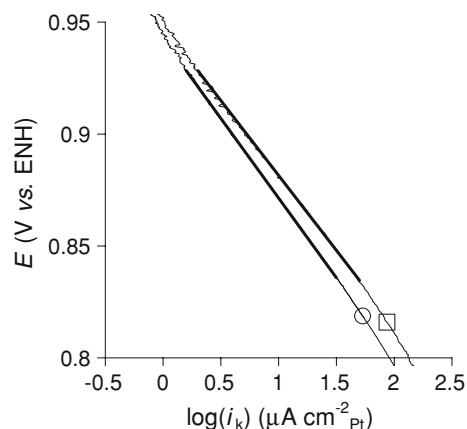
Discussion

No clear significant difference between the two samples can be highlighted by physico-chemical characterization techniques. Both are bidisperse catalysts containing small
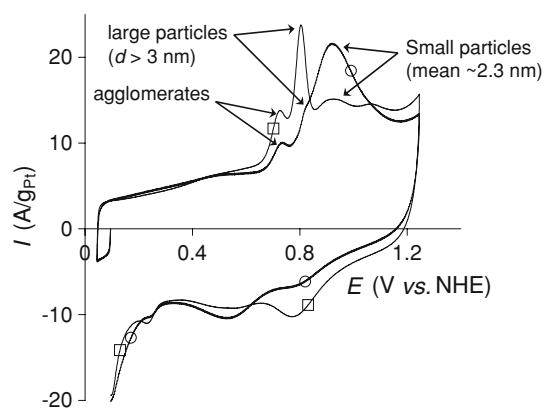
Fig. 4 CO_{ads} stripping voltammogram on the two catalysts in H_2SO_4 (1 M) at 25 °C; sweep rate of 0.02 V s^{-1}. (*circle*) Pt/carbon xerogel; (*square*) Pt/carbon aerogel

Fig. 5 Tafel representation of the ORR voltammograms obtained in H_2SO_4 (1 M) at 25 °C, sweep rate of 10^{-3} V s^{-1}: voltage as a function of the current density corrected from the diffusion–convection in the solution. (*circle*) Pt/carbon xerogel; (*square*) Pt/carbon aerogel

and large Pt particles, in agreement with previous data [8, 9]. In our opinion, the two particle families originate from two different mechanisms of Pt particles formation: (i) the small particles are mostly formed by adsorption of $PtCl_6^{2-}$ anions on the support surface followed by reduction in the adsorbed state, whereas (ii) the large particles are probably originating from the direct reduction of $PtCl_6^{2-}$ anions located in the impregnation solution, followed by metal precipitation on the carbon support.

Indeed, Lambert et al. [24] showed that the adsorption of $PtCl_6^{2-}$ anions onto the carbon surface is limited by a thermodynamic equilibrium. The surface properties of the carbon support are of primary importance for obtaining the desired Pt uptake, dispersion and particle size distribution, since structural defects and functional groups on the carbon surface usually act as nucleation centres for metal deposition. In consequence, the chemical surface state of the support (regulated by the oxygenated surface groups and the pH of the solution) is considered a key parameter. For example, the impregnation of carbon xerogels with H_2PtCl_6 aqueous solution (5 mmol/L) leads to a maximum Pt loading of 8–10 wt%; this result was obtained by fixing the pH of the solution at its optimal value of 2.5 [24]. Modifying the pH reduces the Pt uptake. Increasing the concentration of the solution above 5 mmol L^{-1} does not lead to increased Pt loading of the final catalyst: the excess of Pt complex remains in solution. After filtration, drying and reduction under H_2, the catalyst is well dispersed and

homogeneously distributed: the Pt particles are about 2 nm in diameter without agglomeration. In addition, the meso/macropore size and volume play no role in the adsorption step, and similar results were obtained for carbon gels with equivalent-specific surface areas.

Since the composition of the pristine gels is quite the same, both supports used in this study are very similar in terms of surface chemistry. Carbon xerogels and aerogels obtained by pyrolysis (at 800 °C or above) of dried RF gels contain very few oxygen surface groups [16, 25]; in addition, the point of zero charge of the supports, which is related to the surface chemistry, is in all cases close to 9 [8, 24]. As a consequence, their behaviour towards $PtCl_6^{2-}$ adsorption is believed to be similar. In this study, the pH of the impregnation solution was not fixed at its optimum value but does not forbid adsorption of $PtCl_6^{2-}$. Adding $NaBH_4$ to the slurry yields reduction of both the adsorbed and unadsorbed Pt^{z+} species. As stated above, by comparison with the results obtained after elimination of the solution and reduction under H_2, it seems probable that the small particles are mostly formed by reduction of the adsorbed species, whereas large particles are obtained by precipitation of the metal remaining in the solution. Nevertheless, since the small particles are larger than those observed when the excess of impregnation solution is eliminated [24] ($\sim$4–5 nm instead of $\sim$2 nm), it seems

Table 3 Results from CO_{ads} stripping and ORR voltammetry

Catalyst	$S_{CO\text{-strip}}$ (m^2 g$_{Pt}^{-1}$) $\pm 10\%$	b (V dec^{-1}) $\pm 5\%$	SA_{85} (μA cm$_{Pt}^{-2}$) $\pm 5\%$	SA_{90} (μA cm$_{Pt}^{-2}$) $\pm 5\%$
X-Pt	32	0.072	19.9	3.9
A-Pt	29	0.067	29.0	5.1

$S_{CO\text{-strip}}$ Pt surface area determined using the coulometry in CO_{ads} stripping experiments, b Tafel slope for the ORR, SA_{85} specific activity at $E = 0.85$ V, SA_{90} specific activity at $E = 0.90$ V

that the reduction step in aqueous phase also impacts the Pt nanoparticles formation and final dispersion. This difference could also be explained as follows: the amount of Pt deposited on catalysts A-Pt and X-Pt exceeds by far the maximum obtained by impregnation in the optimal conditions (i.e. 8–10 wt% [24]), which can be detrimental to metal dispersion, even for the small particle group.

Summing up, the results deduced from physico-chemical characterization methods (XRD, CO chemisorption and TEM) do not explain the difference of activity towards oxygen reduction. These techniques give access to the global metal dispersion, but thorough information about the structure of the Pt particles is not easy to deduce, especially in such inhomogeneous catalysts: (i) XRD signal corresponding to small particles is completely overwhelmed by that of the large ones; (ii) CO chemisorption provides only a measurement of the total accessible Pt surface, and the chemisorption stoichiometry depends on the Pt particle size; (iii) since the observation remains quite local and possible only for small grains of the catalyst, TEM images can be unrepresentative of the global catalyst structure. Concerning TEM, the choice of the images is particularly determinant in the case of the characterization of the large particles. Indeed, Fig. 1a, b shows that the large metal particles are not necessarily homogeneously distributed onto the support. It is therefore difficult to obtain quantitative results from such images.

On the contrary, electrochemical characterization by CO_{ads} stripping voltammetry enables detecting significant differences in the particle size distribution of the two samples. In particular, CO_{ads} stripping voltammograms evidence that the mean particle size of isolated Pt particles seems larger for A-Pt than X-Pt. In addition, the fraction of agglomerated Pt particles is larger for A-Pt versus X-Pt. This can explain quantitatively the observed differences in electrocatalytic activity for the ORR. Indeed, it is well known that the specific activity of Pt nanoparticles (i.e. the current produced per Pt surface area unit) strongly decreases with their size [26, 27] and this has been discussed in terms of geometric and/or electronic effects. Within the framework of geometric effects, it was suggested by Kinoshita [27] that the mass-averaged distribution of the (100) and (111) crystal facets, favourable for ORR, is maximal for particle diameter ca. 3.5 nm. Within the framework of electronic effects, the chemisorption energies and the reaction rates are correlated with the d-band shift and occupancy which are the functions of the particle size [28]. So, the differences observed in CO_{ads} stripping voltammetry match well with the differences in catalytic activity: though both samples display equivalent accessible Pt surface (X-Pt: $S_{CO\text{-strip}} = 32$ m^2 g$_{Pt}^{-1}$; A-Pt: $S_{CO\text{-strip}} = 29$ m^2 g$_{Pt}^{-1}$), catalyst A-Pt, which contains a larger fraction of large Pt particles and aggregates, is more active for the ORR than X-Pt in terms of current produced per surface area unit of platinum.

The results obtained suggest that the nanoparticle formation depends on the support porosity. Indeed, the only difference between the two supports is the meso/macropore texture: the carbon aerogel contains a large volume ($V_{>2nm} = 4.5$ cm^3 g^{-1}) of small mesopores (10–25 nm), whereas the carbon xerogel is characterized by a rather small volume ($V_{>2nm} = 1.8$ cm^3 g^{-1}) of larger voids (macropores, 50–85 nm). Although it is not possible to deduce a precise mechanism for the formation of large particles, it is probable that the narrowness of the pores present in the aerogel hampers the accessibility to the whole carbon surface (within the pores) of the Pt species and BH_4^- during the liquid phase reduction step, which would lead to a less homogeneous Pt particle dispersion, and to a bigger amount of large particles.

To estimate the Pt-specific surface area, two approaches were used: gas-phase chemisorption and electrochemical CO_{ads} stripping. The specific surface areas determined by CO_{ads} stripping ($S_{CO\text{-strip}}$) are systematically lower by a factor ca. 20–25% than the surface area determined by CO chemisorption ($S_{CO\text{-chem}}$). Considering that CO adsorbs non-dissociatively on Pt and that Pt particles are stable under CO atmosphere, the above observation implies that either (i) the stoichiometry of CO adsorption is different in gas-phase catalysis or electrocatalysis or (ii) the aqueous electrolyte media does not enter the whole pore volume of the carbon support, leading to detecting <100% of the effective Pt surface area or even (iii) the Pt particles are poisoned by residues coming from the catalyst synthesis or even from the AL elaboration procedure. Regarding the first hypothesis, i.e. the stoichiometry of CO chemisorption, it must be mentioned that the fraction of accessible surface might even be underestimated in gas-phase catalysis due to choice of $X_{Pt\text{-CO}}$. On the one hand, Rodríguez-Reinoso et al. [20] reported that $X_{Pt\text{-CO}}$ equals 1 for particles >5 nm but increases up to 1.61 for smaller Pt particles. This implies that the surface developed by Pt particles <5 nm may have been severely underestimated in this study. On the other hand, for massive poly or single crystalline Pt electrodes, the maximum CO_{ads} coverage, θ_{CO}, in electrocatalysis does not exceed ca. 0.8: according to Gomez et al. [21], for Pt(111), Pt(100) and Pt(110), θ_{CO} equals 0.64, 0.82 and 0.82, respectively. However, higher packing density of CO_{ads} vs. H_{upd} (under-potential deposited hydrogen) has been evoked for particles <3.5 nm [11], the origin of such effect still being unclear [29]. The second hypothesis, i.e. an incomplete wetting of the carbon surface by the electrolyte, seems unlikely. Indeed, the electrochemical response of the carbon support remained stable in cyclic voltammetry under Ar before and after CO_{ads} stripping and ORR kinetics measurements: the current originating from the two

voltammograms shown in Fig. 4 is quite superimposed at the beginning of the cycle while the two supports display very different pore sizes (85 and 25 nm, respectively): should the problem come from incomplete wetting of the support, it seems improbable to observe equal filling of both carbons by the electrolyte. In addition, the outgassing performed prior to the electrochemical characterization was sufficient to ensure a full contact between the carbon internal surface and the electrolyte. Concerning the third hypothesis, Holscher and Sachtler [30] showed that CO is one of the strongest poisons adsorbed on platinum: in the presence of CO, poisons originally adsorbed on the Pt particle surface should be displaced. However, the kinetics of displacing may be too slow to be completed after a few minutes: this would explain why CO chemisorption in gaseous phase, during which equilibrium is reached prior to any gas injection, leads to larger Pt surfaces than CO_{ads} stripping in liquid phase. Another possibility remains the effect of Nafion®, present in the catalyst layer, on the number of electrochemically active Pt sites and this has been discussed previously by Guilminot et al. [22].

Conclusions

The results presented in this study show to what extent electrochemical characterization might complete classical physico-chemical characterization performed on catalysts.

Two Pt/C catalysts were prepared by impregnation of two supports with very different pore texture, one carbon xerogel and one carbon aerogel. The metal particles were first investigated by physico-chemical characterization techniques: XRD, TEM and CO chemisorption. The data obtained showed no significant differences between the two samples. However, CO_{ads} stripping voltammetry enabled detecting structural differences between the catalysts: although the total Pt surface is almost the same, the surfaces of the CO desorption peaks corresponding to Pt particles of various sizes and aggregation state differ drastically, which impacts the catalyst activity towards structure–sensitive reactions, such as oxygen reduction. In addition, CO_{ads} stripping measurements show that a large fraction of the Pt surface detected by CO chemisorption is not accessible to the reactants. This could be due to a catalyst poisoning, undetected by the latter technique.

As a conclusion, electrochemical characterization such as CO_{ads} stripping voltammetry turns out to be very helpful to complete the physico-chemical characterization of catalysts, even though the final application is not electrocatalysis. Indeed, many reactions are structure–sensitive, and differences in catalytic activities could be explained by the detection of structure differences through electrochemical characterization.

References

1. Pekala RW (1989) J Mater Sci 24:3221. doi:10.1007/BF01139044
2. Al-Muhtaseb SA, Ritter JA (2003) Adv Mater 15:101
3. Job N, Théry A, Pirard R et al (2005) Carbon 43:2481
4. Moreno-Castilla C, Maldonado-Hódar FJ (2005) Carbon 43:455
5. Job N, Heinrichs B, Lambert S et al (2006) AIChE J 52:2663
6. Samant PV, Pereira MFR, Figueiredo JL (2005) Catal Today 102–103:183
7. Marie J, Berthon S, Achard P et al (2004) J Non-Cryst Solids 350:88
8. Marie J, Berthon-Fabry S, Chatenet M et al (2007) J Appl Electrochem 37:147
9. Job N, Marie J, Lambert S et al (2008) Energ Convers Manage 49:2461
10. Marie J, Chenitz R, Chatenet M et al (2009) J Power Sources 190:423
11. Maillard F, Eikerling M, Cherstiouk OV et al (2004) Faraday Discuss 125:357
12. Maillard F, Schreier S, Hanzlik M et al (2005) Phys Chem Chem Phys 7:385
13. Maillard F, Savinova E, Stimming U (2007) J Electroanal Chem 599:221
14. Alié C, Pirard R, Lecloux AJ et al (1999) J Non-Cryst Solids 246:216
15. Lecloux AJ (1981) In: Anderson JR, Boudart M (eds) Catalysis, science and technology, vol 2. Springer, Berlin, pp 171–230
16. Job N, Pereira MFR, Lambert S et al (2006) J Catal 240:160
17. Bergeret G, Gallezot P (1997) In: Ertl G, Knözinger H, Weitkamp J (eds) Handbook of heterogeneous catalysis. Wiley, Weinheim, pp 439–464
18. Trasatti S (1992) J Electroanal Chem 327:353
19. Bard AJ, Faulkner LR (1992) Electrochemical methods: fundamentals and applications. Wiley, New York, p 283
20. Rodríguez-Reinoso F, Rodríguez-Ramos I, Moreno-Castilla C et al (1986) J Catal 99:171
21. Gomez R, Feliu JM, Aldaz A et al (1998) Surf Sci 410:48
22. Guilminot E, Corcella A, Chatenet M et al (2007) J Electroanal Chem 599:111
23. Gasteiger HA, Kocha SS, Sompalli B et al (2005) Appl Catal B 56:9
24. Lambert S, Job N, D'Souza L et al (2009) J Catal 261:23
25. Mahata N, Pereira MFR, Suárez-García F et al (2008) J Colloid Interface Sci 324:150
26. Kinoshita K (1988) Carbon—electrochemical and physicochemical properties. Wiley, New York, p 48
27. Kinoshita K (1990) J Electrochem Soc 137:845
28. Henry CR (1998) Surf Sci 31:235
29. Maillard F, Pronkin S, Savinova ER (2009) In: Vielstich W, Gasteiger HA, Yokokawa H (eds) Handbook of fuel cells, Advances in electocatalysis, materials, diagnostics and durability, vol 5. John Wiley & Sons, Inc., New York, pp 91–111
30. Holscher HH, Sachtler WMH (1966) Discuss Faraday Soc 41:29